

Pole analysis on the hadron spectroscopy of $\Lambda_b \rightarrow J/\Psi p K^-$

Shi-Qing Kuang,¹ Ling-Yun Dai,^{1,*} Xian-Wei Kang,² and De-Liang Yao¹

¹*School of Physics and Electronics, Hunan University, Changsha 410082, China*

²*College of Nuclear Science and Technology, Beijing Normal University, Beijing 100875, China*

In this paper we study the $J/\Psi p$ spectroscopy in the process of $\Lambda_b \rightarrow J/\Psi p K^-$. The final state interactions of coupled channel $J/\Psi p - \bar{D}\Sigma_c - \bar{D}^*\Sigma_c$ are constructed based on K-matrix with the Chew-Mandelstam function. We build the $\Lambda_b \rightarrow J/\Psi p K^-$ amplitude according to the Au-Morgan-Pennington method. The event shape is fitted and the decay width of $\Lambda_b \rightarrow J/\Psi p K^-$ is used to constrain the parameters, too. With the amplitudes we extract out the poles and their residues. Our amplitude and pole analysis suggest that the $P_c(4312)$ should be $\bar{D}\Sigma_c$ molecule, the $P_c(4440)$ could be an S-wave compact pentaquark state, and the structure around $P_c(4457)$ is caused by the cusp effect. The future experimental measurement of the decays of $\Lambda_b \rightarrow \bar{D}\Sigma_c K^-$ and $\Lambda_b \rightarrow \bar{D}^*\Sigma_c K^-$ would further help to study the nature of these resonances.

PACS numbers: 11.55.Fv, 11.80.Et,

Keywords: Dispersion relations, Partial-wave analysis

I. INTRODUCTION

The discovery of hidden-charm hadrons $P_c^+(4380)$ and $P_c^+(4450)$ [1] started a new era of hadron physics as they obviously contain at least five quark component $\bar{c}cuud$. Whether they are compact pentaquark states or hadronic molecules or generated by kinematic effect is still not clear. For recent review on the hadronic molecules and multiquark states, we refer to [2–4]. Recently the LHCb experiment made a great progress [5]. The decay events collected now by Run 1 and Run 2 are about nine times more than that of Run 1 analysis. As a result, the bin size has been decreased from 15 to 2 MeV. With the high statistics they found three structures in the $J/\Psi p$ spectrum of $\Lambda_b \rightarrow J/\Psi p K^-$:

$$\begin{aligned} P_c^+(4312) : M &= 4311.9 \pm 0.7_{-0.6}^{+6.8}, \\ \Gamma &= 9.8 \pm 2.7_{-4.5}^{+3.7}, \\ P_c^+(4440) : M &= 4440.3 \pm 1.3_{-4.7}^{+4.1}, \\ \Gamma &= 20.6 \pm 4.9_{-10.1}^{+8.7}, \\ P_c^+(4457) : M &= 4457.3 \pm 0.6_{-1.7}^{+4.1}, \\ \Gamma &= 6.4 \pm 2.0_{-1.9}^{+5.7}, \end{aligned}$$

with all the units being MeV. Then the question is, what inner structure are they? A cornucopia of models have been done to study the property of these resonances [6–21]. Among them, Ref.[12] uses a coupled channel K-matrix formalism to fit to the data around the $P_c(4312)$. In Ref.[21], the Lippmann-Schwinger equations have been used and the one pion exchange and short range scattering potential have been considered. They found a narrow $\Sigma_c^* \bar{D}$ state ($P_c(4380)$). In addition, three more $\Sigma_c^* \bar{D}^*$ molecules have been seen in the analysis. Here we use the Chew-Mandelstam formalism to write the unitary cut in once subtracted dispersion relation, and we fit up to 4.6 GeV to discuss the three resonances listed

above ($P_c(4312)$, $P_c(4440)$, and $P_c(4457)$). It is worth to point out that the pole counting rule[22, 23] is useful to distinguish the molecule and non-molecule structure. Indeed the shadow poles (not only the ones being closest to the physical sheet) are also important to discuss the inner structure. Our amplitudes around $P_c(4440)$ and $P_c(4457)$ are in high quality and they are helpful for discussing the structure. These will be discussed in next sections.

To extract the information of these resonances, we need amplitude analysis to describe the invariant mass spectroscopy of $\Lambda_b \rightarrow J/\Psi p K^-$. The final state interactions (FSI) are important to be considered. There have been lots of papers that indicate the importance of the FSI, see e.g. [24–32]. We will use the Au-Morgan-Pennington (AMP) method [24] to include the FSI of $J/\Psi p - \bar{D}\Sigma_c - \bar{D}^*\Sigma_c$ triple channels. From the amplitudes we extract out the pole information and discuss their property according to the pole counting rule.

This paper is organized as follows: In Sect. II we use K-matrix to build the hadronic scattering amplitudes of $J/\Psi p - \bar{D}\Sigma_c - \bar{D}^*\Sigma_c$ triple channels. The $\Lambda_b \rightarrow J/\Psi p K^-$ amplitude is constructed by AMP method. In Sect. III we fit to the event shape and decay width of $\Lambda_b \rightarrow J/\Psi p K^-$ and determine the parameters. The amplitudes are continued into un-physical Riemann sheets (RSs) and the poles in different RSs are extracted out. By pole analysis the origin of these poles are discussed. In Sect. IV we discuss the fits to other datasets given by LHCb. We end with a brief summary.

II. DECAY AMPLITUDE

To get the information of poles, we need an amplitude analysis to get accurate hadronic scattering amplitudes. The following problem is which channel should be included? As is predicted in [33, 34], there could be $\bar{D}\Sigma_c$ and $\bar{D}^*\Sigma_c$ hadronic molecule states with quantum number $IJ^P = \frac{1}{2}\frac{1}{2}^-$ at $4261 + i28.5$ and $4412 + i23.6$ MeV of each channel. This is later studied in [35] by a cou-

*Electronic address: dailiingyun@hnu.edu.cn

pled channel unitary approach. In Ref.[5], the $P_c^+(4312)$ is found to be under $\bar{D}\Sigma_c$ threshold and more like an S-wave resonance. The other two resonances are proximate to the $\bar{D}^*\Sigma_c$ threshold. We thus take $J/\Psi p - \bar{D}\Sigma_c - \bar{D}^*\Sigma_c$ as the coupled channels. The helicity has been ignored as that the heavy quark spin symmetry ensures the spin-dependent interactions related to the heavy quark are of the order of $1/m_Q$ [36]¹. This assumption is consistent with the analysis of Ref.[5], where it is found that including P-wave factors in the Breit-Wigner amplitudes has negligible effect on the results. We construct our amplitude based on K-Matrix to keep unitarity, and have

$$T(s) = K(s)[1 - C(s)K(s)]^{-1}, \quad (1)$$

where \sqrt{s} is the energy in the center of mass frame. $K(s)$ is a real matrix. $C(s)$ is the diagonal matrix of the canonical definition of Chew-Mandelstam functions [37, 38], and it could be written in once subtracted dispersion relation:

$$C_i(s) = \frac{s}{\pi} \int_{s_{thi}}^{\infty} ds' \frac{\rho_i(s')}{s'(s' - s)}, \quad (2)$$

where $i(j) = 1, 2, 3$ represent for $J/\Psi p$, $\bar{D}\Sigma_c$, $\bar{D}^*\Sigma_c$, respectively, with isospin 1/2. $s_{thi} = (M_i + m_i)^2$ is the threshold and M_i (m_i) is the mass of meson (baryon) in the i -th channel. The phase space factor has only diagonal elements:

$$\rho_i(s) = \sqrt{\frac{(s - (M_i + m_i)^2)(s - (M_i - m_i)^2)}{s^2}}. \quad (3)$$

The Chew-Mandelstam function could be expressed explicitly as

$$C_i(s) = \frac{1}{\pi} + \frac{M_i^2 - m_i^2}{\pi s} \ln\left(\frac{m_i}{M_i}\right) - \frac{M_i^2 + m_i^2}{\pi(M_i^2 - m_i^2)} \ln\left(\frac{m_i}{M_i}\right) + \frac{\rho_i(s)}{\pi} \ln\left(\frac{\sqrt{(M_i + m_i)^2 - s} - \sqrt{(M_i - m_i)^2 - s}}{\sqrt{(M_i + m_i)^2 - s} + \sqrt{(M_i - m_i)^2 - s}}\right). \quad (4)$$

The new high statistics results of $J/\Psi p$ line shape (in the process of $\Lambda_b \rightarrow J/\Psi p K^-$) from LHCb [5] help us to constrain the hadronic scattering amplitude. To describe it, the rescattering of inelastic channels ($\bar{D}\Sigma_c$, $\bar{D}^*\Sigma_c$) needs to be considered. We implement the AMP formalism [24] to include the FSI:

$$F_i(s) = \sum_{k=1}^3 \alpha_k(s) T_{ki}(s), \quad (5)$$

where ‘ i ’ has the same meaning as explained after Eq. (2). The $\alpha_i(s)$ are polynomials of s , absorbing all the contributions of left hand cut and distant right hand cut. For

simplicity we set them to be constant $\alpha_{1,2,3}$ and ignore higher order terms. It is easy to check that Eq. (5) satisfies the final state interactions theorem:

$$\text{Im}F_i(s) = \sum_{k=1}^3 F_k^* \rho_k(s) T_{ki}(s). \quad (6)$$

With this amplitude we fit to the invariant mass spectroscopy

$$\frac{d\Gamma_i}{d\sqrt{s}} = \frac{\lambda^{1/2}(s, M_{J/\Psi}^2, m_p^2) \lambda^{1/2}(M_{\Lambda_b^0}^2, s, m_K^2) |F_i|^2}{256\pi^3 M_{\Lambda_b^0}^3 \sqrt{s}}. \quad (7)$$

Here the Källén function λ is defined as $\lambda(x, y, z) = (x - y - z)^2 - 4yz$. To fit to the invariant mass spectroscopy one would need to time $\frac{d\Gamma_i}{d\sqrt{s}}$ with a normalization factor ‘ N ’. The decay width given by the PDG [39] could be used to constrain the α_i , too. But still we lack adequate constraints on $F_2(s)$ and $F_3(s)$ amplitudes. Indeed in Ref.[17], the ratio of the coupling constants $\frac{g_{P_c(4306)\bar{D}\Sigma_c}}{g_{P_c(4306)J/\Psi p}}$ and $\frac{g_{P_c(4453)\bar{D}^*\Sigma_c}}{g_{P_c(4453)J/\Psi p}}$ are roughly 4 and 2 times, while the ratios of the phase spaces (with $F_i(s) = 1$ in Eq. (7)) are $PS_2/PS_1 \simeq 0.6, 0.4$, respectively. This suggests that the branching ratios of Br_2 ($\Lambda_b^0 \rightarrow \bar{D}\Sigma_c K^-$) and Br_3 ($\Lambda_b^0 \rightarrow \bar{D}^*\Sigma_c K^-$) could be the same order as that of Br_1 ($\Lambda_b^0 \rightarrow J/\Psi p K^-$). We thus make the ‘data’ as $\text{Br}_{2,3} = \text{Br}_1$, and the uncertainty of $\text{Br}_{2,3}$ is set to be 10 times as the central values of them. We input these as constraints.

III. FITTING STRATEGY AND POLE ANALYSIS

For K matrix, we try to use as less parameters as possible. Only when more parameters are indispensable to reduce the χ^2 distinctly do we include them. A pole² in the K matrix is necessary to fit to the event shape around $P_c(4440)$. Adding a P-wave instead of inputting a K matrix pole is also checked. It is somehow helpful to distinguish the quantum number of $P_c(4440)$. For the P-wave scattering amplitude we adopt the Blatt-Weisskopf barrier factor representation [27], see the supplement for details. The following fits are performed:

- 1) **Fit 1:** We do not include any poles in the K matrix. $\chi_{\text{d.o.f}}^2 = 1.41$.
- 2) **Fit 2:** As in Fit 1 but we include one pole in the K matrix. $\chi_{\text{d.o.f}}^2 = 1.32$.
- 3) **Fit 3:** As in Fit 1 we do not include poles in the K matrix, but add a P-wave instead. $\chi_{\text{d.o.f}}^2 = 1.32$.

¹ We are aware of that the spin dependent interactions between the light quarks can not be ignored, and we refer readers to read Ref.[21].

² We tried to input more poles in the K matrix, but it only helps to improve the fit a little and will not change the conclusion here.

The parameters of all the fits are shown in the supplement. The fit results are shown in Fig. 1. Our amplitudes fit well to the high statistics LHCb data in 2019 [5], with $\cos\theta_{P_c}$ weighted. It is worth to point out that this dataset has removed much of the interfering of the Λ^* , which is in the K^-p channel and most populated at $\cos\theta_{P_c} > 0$. Owing to this our K matrix fit without three body final state interactions is feasible. The branching ratios of Br_1 is exactly the same as that of PDG, and in most of the fits the Br_2 is of 10^{-4} , and Br_3 is of 10^{-5} . Notice that in Fit 1 it does not have the structure around the $\sqrt{s} = 4440$ MeV.

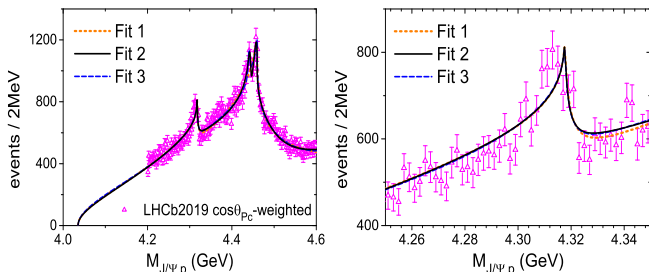


FIG. 1: Fits to the $J/\Psi p$ spectroscopy of $\Lambda_b \rightarrow J/\Psi p K^-$. The right graph is enlarged around the $P_c(4312)$. The LHCb 2019 data is the $\cos\theta_{P_c}$ -weighted one from Ref. [5].

To study the resonances we enlarge the size of the plots around the structures, as shown in Fig. 2 and the right side graph of Fig. 1. For the $P_c(4312)$, our amplitude fits

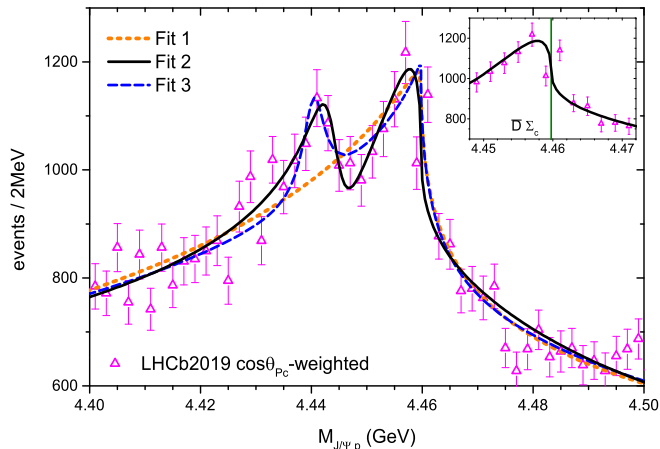


FIG. 2: Fit of the $J/\Psi p$ spectroscopy of $\Lambda_b \rightarrow J/\Psi p K^-$ for enlarged size around $P_c(4440)$ and $P_c(4457)$.

to the data well. Though the amplitude is a bit lower than the data on the left side of the ‘peak’, it is within the margin of the data error. Note that we do not input a K-matrix pole around $P_c(4312)$ in the K-matrix formalism. This is why our ‘peak’ exactly locates at the $\bar{D}^*\Sigma_c$ threshold ($\sqrt{s} = 4.3177$ GeV), shifting a bit to the right side of the peak of the data. For the $P_c(4440)$, our Fits 2 and 3 fit to the data well, while in Fit 1 one can not find such a structure. This is caused by that in Fit 1 we do not include the K matrix pole in $\bar{K}(s)$. As shown in Fig.2, the Fit 2 is better than Fit 3 in both the $P_c(4440)$ and the $P_c(4457)$ region. Our results prefer an S-wave

$P_c(4440)$. For the $P_c(4457)$, our amplitude behaves more like a cusp caused by the $\bar{D}^*\Sigma_c$ threshold effect. These will be discussed in next sections.

With the amplitudes given by the Chew-Mandelstam formalism, the information of the poles can be extracted out. We continue the $T(s)$ amplitude to the unphysical Riemann sheets based on unitarity and analyticity. The definition of the Riemann sheet (RS) could be found in [40]. Here we use the following definition [41] as shown in Table I. The pole s_R and its coupling/residue of the

	I	II	III	IV	V	VI	VII	VIII
ρ_1	+	-	-	-	+	+	-	+
ρ_2	+	+	-	-	-	+	+	-
ρ_3	+	+	+	-	+	-	-	-

TABLE I: The sign of phase factors for each Riemann sheet.

RS-n in the triple channel are defined as:

$$T_{ij}^n(s) = \frac{g_i g_j}{s_R^n - s}, \quad (8)$$

where the subscript ‘ i, j ’ denotes the hadronic channels as before. The poles in different RSs for all the fits are given in Table II. In Fit 1, we only find poles of $P_c(4312)$.

State	pole locations (MeV)					
	RS	Fit.1	RS	Fit.2	RS	Fit.3
$P_c(4312)$	III	$4296.93^{+2.48}_{-3.00}$ $-i5.12^{+2.44}_{-1.06}$	III	...	V*	$4313.38^{+2.52}_{-5.73}$ $-i2.05^{+1.65}_{-0.75}$
	V*	$4312.74^{+1.69}_{-0.67}$ $-i3.33^{+2.91}_{-1.25}$	V*	$4314.31^{+2.06}_{-1.10}$ $-i1.43^{+1.50}_{-0.57}$	VIII	$4313.11^{+3.86}_{-4.76}$ $-i3.11^{+1.63}_{-2.02}$
$P_c(4440)$	III*	$4444.09^{+2.53}_{-1.48}$ $-i3.10^{+0.53}_{-1.33}$	III*	$4440.53^{+0.47}_{-0.31}$ $-i2.42^{+0.22}_{-0.22}$
	IV	$4443.69^{+2.89}_{-1.34}$ $-i0.32^{+1.23}_{-0.04}$	IV	$4440.38^{+0.41}_{-0.19}$ $-i1.40^{+0.59}_{-0.50}$
	V	$4444.22^{+2.72}_{-1.41}$ $-i2.48^{+0.57}_{-0.67}$	V	$4440.53^{+0.37}_{-0.30}$ $-i2.32^{+0.27}_{-0.61}$
	VII	$4443.84^{+1.93}_{-1.91}$ $-i1.02^{+1.05}_{-0.92}$	VIII	$4440.38^{+3.31}_{-0.52}$ $-i1.30^{+4.45}_{-0.50}$
	III	$4466.53^{+2.13}_{-4.75}$ $-i3.88^{+6.95}_{-0.93}$
	VII	$4456.77^{+3.10}_{-8.89}$ $-i7.77^{+11.07}_{-4.41}$	VIII	$4453.44^{+7.11}_{-3.34}$ $-i21.58^{+8.01}_{-6.36}$

TABLE II: The pole locations given by our fits. The Riemann sheets with bold type and the ‘*’ symbol means that they are close to the physical sheet.

And in Fits 2 and 3 we find poles of all the three resonances. Fit 2 describes the data better with less assumptions, we choose it as our optimistic one. To classify the inner structure of the poles, we use the ‘criteria’ proposed

in Ref. [22, 41]: A triple channel Breit-Wigner resonance should appear as quadruplet poles in different RSs, while a molecule has less poles.

$P_c(4312)$

This resonance (pole) is rather stable in all the fits. We can find it without an input pole in the $K(s)$. The poles locate at the RS-III and/or V. For each fit we can find only one or two poles. According to the ‘pole counting’, it is a $\bar{D}\Sigma_c$ molecule. The masses of the poles are a bit below the threshold $\sqrt{s_{th2}} = 4317.73$ MeV, and their widths (2 times of the imaginary part of the pole) are only a few MeV. This supports the molecule picture. As is known, RS-II and III are the closest sheet to the physical one below and above $\bar{D}\Sigma_c$ threshold, respectively. RS-II and RS-V are connected along the unitary cut above the $\bar{D}\Sigma_c$ threshold. The shadow poles appear in RS-V but not in RS-II suggests that there is a strong dynamics to drag the pole from RS-II to RS-V. The pole in RS-III confirms such observation. This is consistent with the molecule picture, as our interaction between the resonance and the $\bar{D}\Sigma_c$ is strong, this is typical way how a virtual state (with weak interaction to the $\bar{D}\Sigma_c$) changes into a molecule. For the strength of the couplings please see the $|g_2|$ of Table A.4, in the Appendix.

$P_c(4440)$

The masses of the poles are quite close to the input K matrix pole 4443.60 MeV in Fit 2. These poles are found in four sheets: RS-III, IV, V, VII/VIII, being close to each other. The widths are quite narrow and the poles are quite close to the real axis. According to ‘pole counting’, it is an elementary particle. Since it decays into $J/\Psi p$ and have five quark component, this implies a compact pentaquark picture. Note that our widths of the $P_c(4440)$ are small. Indeed in all our fits except for Fit 1, including Fits A, B and C, all the $P_c(4440)$ have small widths, see also Table A.3 in the Appendix. And all of our fits describe the blow-up of the data in the $P_c(4440)$ region well. If neither the pole in K matrix nor the higher partial wave resonance is input, one can not obtain such a blow-up (Fit 1). Obviously the kinematic behaviour can not supply such a structure. This supports the compact pentaquark picture. For its quantum number, in Refs.[8, 33–35], they suggest $P_c(4440)$ to be $1/2^-$, while in Refs.[20, 42], they suggest $3/2^-$. In our case, Fit 3 is worse than Fit 2 and we prefer the $P_c(4440)$ to be S-wave, but it is not possible to distinguish the quantum number.

$P_c(4457)$

We do not find poles in Fit 1, and find poles in RS-III and VII in Fit 2 and a pole in RS-VIII in Fit 3. For RS-VII and VIII they are faraway from the physical region. Absence of poles close to the physical region means that the structure is caused by cusp effect. The pole in RS-III (Fit 2) is 7 MeV above the threshold $\sqrt{s_{th3}} = 4459.75$ MeV, barely close to the physical region. From the ‘pole counting’ it does not support the molecule or ‘Breit-Wigner’ types, but a molecular component can not be entirely excluded in Fit 2. In the region around $\bar{D}^*\Sigma_c$, our amplitude behaves more like a cusp but not a normal Breit-Wigner structure. In Fits 1 and 3 they are caused by cusp effect and in Fit 2 there is a sharp decline near the $\bar{D}^*\Sigma_c$ threshold, see the graph in the top-right corner of Fig.2. Indeed, this structure is very similar to that of the

$\eta'\pi^+\pi^-$ line shape around $\bar{p}p$ threshold, see Fig.4 of [43] and Fig.4 of [44].

IV. ANALYSIS OF OTHER DATASETS

We also check the case that we fit to other datasets given in Ref. [5], the ‘ m_{Kp} all’ and the ‘ $m_{Kp} > 1.9$ GeV’ ones. In all these fits the treatment with the background is different, but the pole information should be model independent. Following it, these fits could be used to check the reliability of our amplitude analysis. The following extra fits are performed:

- 1) **Fit A:** As in Fit.2 but we fit to the data of ‘ m_{Kp} all’ case (without requiring $m_{Kp} > 1.9$ GeV).
- 2) **Fit B:** As in Fit.2 but we fit to the data with requiring $m_{Kp} > 1.9$ GeV.
- 3) **Fit C:** As in Fit.2 we fit to the data with requiring $\cos\theta_{P_c}$ weighted, with the isospin symmetry violation included.

The invariant mass spectrum is given in Fig.3. Notice that in Fit C, with isospin violation included, it fits better to the data near thresholds.

The discussion of the event shape structure of these fits are consistent with that given by Fits 1, 2, and 3. In each fit, there are only one or two poles in RS-III and/or V of the $P_c(4312)$. It supports the molecular component. And there are four poles of the $P_c(4440)$ in RS-III, IV, V, VII/VIII. They are close to each other and the widths are narrow. This supports the compact pentaquark component. For the $P_c(4457)$ we do not find poles nearby in Fits A and B but find two poles in RS-III and VII in Fit C. Our line shape falls down obviously near the $\bar{D}^*\Sigma_c$ threshold in Fits A and C. And in Fit B ours exhibits a pronounced cusp-like structure around the $\bar{D}^*\Sigma_c$ threshold. These confirm the cusp effect origin of the $P_c(4457)$, but a component of $\bar{D}^*\Sigma_c$ molecule can’t be excluded. This component could be generated by a virtual state in the $\bar{D}^*\Sigma_c$ single channel scattering nearby the threshold, see Ref.[45] and discussions of the pole trajectory in the supplement.

V. SUMMARY

In this paper we perform an amplitude analysis in the process of $\Lambda_b \rightarrow J/\Psi p K^-$. The $J/\Psi p - \bar{D}^0\Sigma_c^+ - \bar{D}^{*0}\Sigma_c^+$ triple channel scattering amplitude is constructed by K-matrix, within Chew-Mandelstam formalism. Based on it we apply the Au-Morgan-Pennington method to study the process of $\Lambda_b \rightarrow J/\Psi p K^-$, taking into account the final state interactions. Qualified fits to the invariant mass spectroscopy [5] is obtained from $J/\Psi p$ threshold up to $\sqrt{s} = 4600$ MeV. We extract out the poles (Fit 2) and find that the $P_c(4312)$, with the pole location $4314.31^{+2.06}_{-1.10} - i1.43^{+1.50}_{-0.57}$ MeV, should have $\bar{D}\Sigma_c$ molecule component. The $P_c(4440)$, $4444.09^{+2.53}_{-1.48} - i3.10^{+0.53}_{-1.33}$ MeV

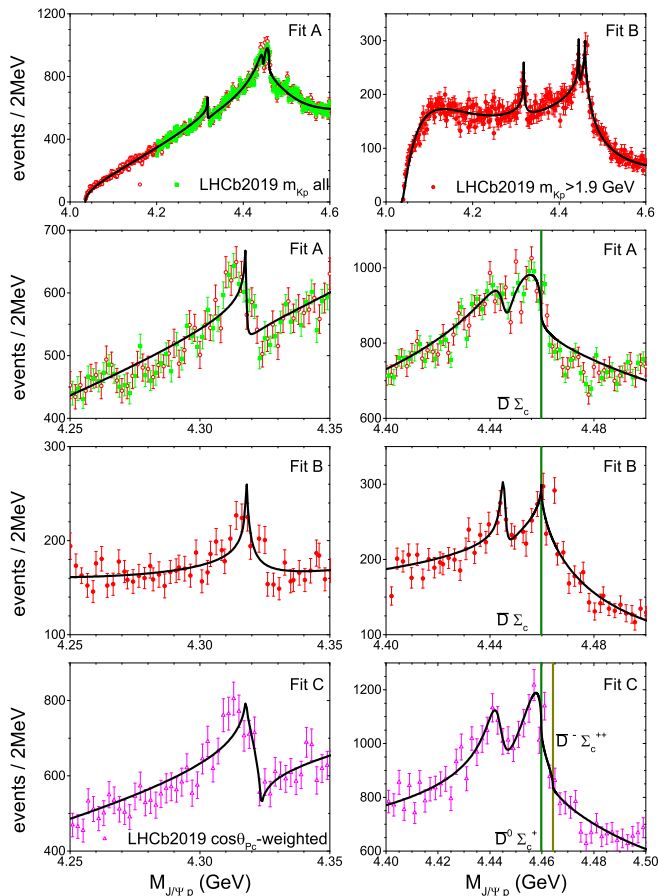


FIG. 3: Fit of the $J/\Psi p$ spectroscopy of $\Lambda_b \rightarrow J/\Psi p K^-$. All the datasets are from Ref. [5]. In Fit A the data is from the ‘ m_{Kp} all’ case, where the red open circle is from Fig.1 and green square is from Fig.3 of Ref. [5]. In Fit B the data is from the ‘ $m_{Kp} > 1.9$ GeV’ case. In Fit C the data is from the $\cos\theta_{P_c}$ -weighted one. The vertical lines denote the $\bar{D}^* \Sigma_c$ thresholds.

in RS-IV, prefers to be a compact S-wave pentaquark. The $P_c(4457)$ is most likely to be caused by cusp effect, while a component of $\bar{D}^* \Sigma_c$ molecule can’t be excluded. We also predict the branching ratios (Fit 2) of the decay of $\Lambda_b^0 \rightarrow \bar{D} \Sigma_c K^-$ and $\Lambda_b^0 \rightarrow D^* \Sigma_c K^-$ as $(1.49 \pm 0.26) \times 10^{-4}$ and $(0.30 \pm 0.08) \times 10^{-4}$, respectively. The future LHCb measurement of the decays, for instance $\Lambda_b^0 \rightarrow D^- \Sigma_c^{++} K^-$ and $\Lambda_b^0 \rightarrow D^{*-} \Sigma_c^{++} K^-$, will tell us further information about these mysterious resonances.

VI. ACKNOWLEDGEMENTS

We are grateful to Profs. Li-Sheng Geng, Feng-Kun Guo and Han-Qing Zheng for their suggestions. Helpful Discussions with Jie-Sheng Yu and Li-Ming Zhang (member of LHCb collaboration) are also acknowledged. This work is supported by National Natural Science Foundation of China (NSFC) with Grant Nos.11805059, 11805012, 11905258. Joint Large Scale Scientific Facil-

ity Funds of the NSFC and Chinese Academy of Sciences (CAS) under Contract No.U1932110, and Fundamental Research Funds for the Central Universities.

Appendix A: K matrix formalism

The real K matrix $K(s)$ could be parametrized as

$$K^{ij}(s) = \sum_l \frac{f_l^i f_l^j}{(s_l - s)} + \sum_{n=0} c_n^{ij} \left(\frac{s}{s_{th1}} - 1 \right)^n. \quad (\text{A.1})$$

To reduce the model dependence, we include as less as possible parameters. According to practice we set $c_{n \geq 2}^{ij} =$

0 and $s_{l \geq 2} = 0$. In Fits A and B we apply the same method as that of Fit 2. In Fit C we take into account the contribution of isospin violation, where the phase space factor $\rho_2(s)$ is replaced by $\frac{1}{2}[\rho_{D-\Sigma_c^{++}}(s) + \rho_{\bar{D}^0 \Sigma_c^+}(s)]$, and so on for $\rho_3(s)$. See Ref.[25] for similar discussions on isospin symmetry breaking in $\overline{K}K$.

The parameters and $\chi^2/d.o.f$ of all our fits are given in Table A.1.

	Fit 1	Fit 2	Fit 3	Fit A	Fit B	Fit C
$s_1(\text{GeV}^2)$...	19.7305 ± 0.01080	...	19.7320 ± 0.0021	19.6418 ± 0.0054	19.7305 ± 0.01132
$f_1^1(\text{GeV})$...	0.0383 ± 0.0099	...	0.0710 ± 0.0065	-0.3539 ± 0.0101	0.0462 ± 0.0131
$f_1^2(\text{GeV})$...	-0.0890 ± 0.0140	...	-0.0873 ± 0.0069	0.2660 ± 0.0072	-0.0704 ± 0.0127
$f_1^3(\text{GeV})$...	0.0670 ± 0.0093	...	0.0801 ± 0.0046	0.2434 ± 0.0070	0.0583 ± 0.0069
c_0^{11}	-0.5392 ± 0.1364	-0.9241 ± 0.1060	-0.2112 ± 0.0167	-0.8246 ± 0.0044	0.2132 ± 0.0383	-1.0088 ± 0.0857
c_1^{11}	0.1001 ± 0.0891	1.3494 ± 0.3334	-0.7066 ± 0.0399	1.1965 ± 0.0110	2.7235 ± 0.2104	1.5565 ± 0.3370
c_0^{12}	0.0396 ± 0.0617	0.2071 ± 0.0761	-0.4497 ± 0.908	0.2615 ± 0.0092	-0.8442 ± 0.0009	0.1904 ± 0.0795
c_1^{12}	-4.7656 ± 0.2428	-5.1328 ± 0.4706	1.1062 ± 0.4885	-4.8447 ± 0.0794	-1.2281 ± 0.0726	-5.5531 ± 0.4805
c_0^{22}	-0.4085 ± 0.0554	-0.3649 ± 0.1025	1.1611 ± 0.2074	-0.3118 ± 0.0119	2.1457 ± 0.0083	-0.5259 ± 0.1828
c_1^{22}	9.9884 ± 0.1046	7.8723 ± 0.3215	1.9002 ± 1.5049	7.1725 ± 0.0359	-4.2733 ± 0.1219	7.5295 ± 0.7121
c_0^{13}	-0.7807 ± 0.2070	-0.0407 ± 0.0677	-1.0142 ± 0.0505	-0.3276 ± 0.0301	-0.7798 ± 0.0106	-0.1177 ± 0.0430
c_1^{13}	0.4087 ± 0.8399	-1.6132 ± 0.2264	2.1896 ± 0.2172	0.3794 ± 0.1622	-1.2419 ± 0.0700	-1.0096 ± 0.1143
c_0^{23}	-0.7556 ± 0.1362	-1.0730 ± 0.0402	-0.3413 ± 0.0915	-1.0787 ± 0.0026	-0.5174 ± 0.0024	-1.1652 ± 0.0260
c_1^{23}	0.2857 ± 0.5907	2.6465 ± 0.2148	2.0355 ± 0.4893	2.5469 ± 0.0126	3.7056 ± 0.0416	3.3315 ± 0.1592
c_0^{33}	1.1530 ± 0.1339	1.9358 ± 0.1432	-0.7824 ± 0.0541	1.9411 ± 0.0022	2.8976 ± 0.0005	2.4978 ± 0.1019
c_1^{33}	0.4160 ± 0.4285	-1.7578 ± 0.5785	9.2785 ± 0.2918	-1.3144 ± 0.0359	-3.3015 ± 0.0220	-4.0641 ± 0.3509
$10^6 \alpha_1$	3.8552 ± 0.1107	4.8465 ± 0.1148	9.0434 ± 0.4427	5.2785 ± 0.0305	9.9157 ± 0.0239	4.5698 ± 0.0713
$10^6 \alpha_2$	2.7388 ± 0.1961	3.1546 ± 0.1314	1.6652 ± 0.0709	2.8896 ± 0.0302	9.2770 ± 0.1143	3.3063 ± 0.0673
$10^6 \alpha_3$	2.3640 ± 0.1966	1.5606 ± 0.0743	3.2539 ± 0.2474	1.4212 ± 0.0126	3.0010 ± 0.0522	1.2716 ± 0.1203
$10^{-18} N$	3.4010 ± 0.1292	3.7216 ± 0.2288	3.9913 ± 0.1251	3.8282 ± 0.0102	0.7954 ± 0.0208	3.6896 ± 0.1564
M_P (GeV)	4.4405 ± 0.0006
$\Gamma_{P \rightarrow 1}$ (MeV)	0.1001 ± 0.0170
$\Gamma_{P \rightarrow 2}$ (MeV)	3.7321 ± 1.5880
$\Gamma_{P \rightarrow 3}$ (MeV)	1.0234 ± 0.4089
β_P	1.1771 ± 0.3005
$\chi_{d.o.f}^2$	1.41	1.32	1.32	1.32	1.45	1.23

TABLE A.1: Results of our fits, as explained in the text. The c_0^{ij} is dimensionless and the c_1^{ij} is in unit of GeV^{-2} . The uncertainty of the parameters is given from MINUIT.

For all the fits, the masses of the resonances are given by the PDG [36], and the central values are input as: $M_{\Lambda_b^0} = 5619.60$ MeV, $M_{J/\psi} = 3096.90$ MeV, $M_p = 938.27$ MeV, $M_{\bar{D}^0} = 1864.83$ MeV, $M_{\bar{D}^{*0}} = 2006.85$ MeV, $M_{\Sigma_c^+} = 2452.90$ MeV. We also try to vary the input masses within the uncertainty given by the PDG and find that the fit results change little. In Fit C we also input $M_{\bar{D}^-} = 1869.65$ MeV, $M_{\bar{D}^{*-}} = 2010.26$ MeV, $M_{\Sigma_c^{++}} = 2453.97$ MeV.

To include the P-wave scattering amplitude we adopt

the Blatt-Weisskopf barrier factor representation [25]

$$g_i^2(s) = \frac{M_P \Gamma_{P \rightarrow i} \mathcal{Q}_i(M_P^2)}{\rho_i(M_P^2) \mathcal{Q}_i(s)}, \quad (\text{A.2})$$

with $\mathcal{Q}_i(s) = 1 + q^2/(s - (m_i + M_i)^2)$ and q is chosen to be 1 GeV. Here M_P and $\Gamma_{P \rightarrow i}$ are the input mass and width (decaying to the i -th channel) of the P-wave

resonance in order. We have the scattering amplitudes

$$T^P_i = \frac{g_i(s)^2}{M^2 - s - i\rho_1(s)g_1^2(s) - i\rho_2(s)g_2^2(s) - i\rho_3(s)g_3^2(s)}, \quad (\text{A.3})$$

and the relative Λ_b^0 decay amplitudes

$$\mathcal{F}_i^P = \frac{\beta_P g_i(s)}{M^2 - s - i\rho_1(s)g_1^2(s) - i\rho_2(s)g_2^2(s) - i\rho_3(s)g_3^2(s)}. \quad (\text{A.4})$$

Note that the partial wave decomposition factor and the coupling $g_{P\Lambda_b^0 K^+}$ is absorbed into the β_P .

The branching ratios of all the fits are shown in Table A.2. In all the fits our $\text{Br}_1(\Lambda_b^0 \rightarrow J/\Psi p K^-)$ is ex-

	10^4Br_1	10^4Br_2	10^4Br_3
Fit 1	3.20 ± 0.27	1.22 ± 0.15	0.84 ± 0.19
Fit 2	3.20 ± 0.40	1.49 ± 0.26	0.30 ± 0.08
Fit 3	3.20 ± 0.64	2.04 ± 0.89	4.82 ± 1.20
Fit A	3.21 ± 0.31	0.76 ± 0.08	0.65 ± 0.13
<i>Fit B</i>	3.20 ± 0.31	9.12 ± 0.70	0.63 ± 0.06
Fit C	3.20 ± 0.36	1.73 ± 0.27	0.15 ± 0.04

TABLE A.2: The $\text{Br}_{1,2,3}$ denotes the branching ratios of $\Lambda_b^0 \rightarrow J/\Psi p K^-$, $\Lambda_b^0 \rightarrow \bar{D}\Sigma_c K^-$, $\Lambda_b^0 \rightarrow \bar{D}^*\Sigma_c K^-$, respectively. The PDG [36] value of the branching ratio of $\Lambda_b \rightarrow J/\Psi p K^-$ is $(3.2 \pm 0.6) \times 10^{-4}$.

actly the same as that of PDG, while in most of fits $\text{Br}_2(\Lambda_b^0 \rightarrow \bar{D}\Sigma_c K^-)$ is roughly 1/3 to 2/3 of Br_1 , and the $\text{Br}_3(\Lambda_b^0 \rightarrow \bar{D}^*\Sigma_c K^-)$ is of the order of 10^{-5} . The branching ratio Br_3 of Fit 3 is much different from those of other fits. Notice that in Fit 3 we include the P-wave. This indicates that measuring the $\text{Br}_{2,3}$ would be rather important for the amplitude analysis. Nevertheless, all the $\text{Br}_{2,3}$ are of the order of $10^{-4} - 10^{-5}$. The uncertainty of the branching ratios is collected by the uncertainty from MINUIT and the statistics of a dozen of other solutions. We are aware that the amplitude above $\sqrt{s} = 4.6$ GeV is not fitted to the data. However, as we have checked, using a polynomial to fit to the data above 4.6 GeV and input it in the integration of Eq. (7), the difference is only several percents, at most 11%. We thus use our K matrix amplitude to do the integration in the whole energy region, and input the difference discussed above as part of the uncertainty. Notice that the branching ratios in Fit B do not have the credibility as our other results. This is reflected by the italic type. The reason is that the cut condition $m_{Kp} > 1.9$ GeV reduces the event, and the cut out one should also contribute to the branching ratio. In contrast, the $\cos\theta_{P_c}$ -weighted data has also cut out the Λ^* contribution, but the event shape of it is quite the same as that of the ‘ m_{Kp} all’ data by multiplying a normalization factor. The latter data does not miss such contribution.

The poles and couplings are shown in Tables A.3 and A.4, respectively. For the $P_c(4312)$, we only find one pole in RS-V of Fits A and B. This convince the molecule picture of this resonance. Roughly, in each Fit the residue coupling to $\bar{D}\Sigma_c$ (g_2) is much larger than that coupling to $J/\Psi p$ (g_1). This supports the ‘ $\bar{D}\Sigma_c$ ’ molecule picture,

State	pole locations (MeV)					
	RS	Fit.A	RS	Fit.B	RS	Fit.C
$P_c(4312)$	III	$4320.49^{+0.68}_{-1.37}$ $-i0.38^{+0.31}_{-0.13}$
	V*	$4317.44^{+0.17}_{-0.17}$ $-i0.09^{+0.07}_{-0.01}$	V*	$4316.50^{+0.02}_{-0.02}$ $-i0.003^{+0.001}_{-0.001}$	V*	$4320.74^{+0.64}_{-4.59}$ $-i0.66^{+1.34}_{-0.42}$
$P_c(4440)$	III*	$4445.81^{+0.80}_{-4.43}$ $-i2.77^{+1.09}_{-0.81}$	III*	$4445.46^{+3.34}_{-8.78}$ $-i1.13^{+1.35}_{-0.39}$	III*	$4443.65^{+1.14}_{-1.51}$ $-i3.50^{+0.69}_{-1.44}$
	IV	$4443.86^{+1.41}_{-1.64}$ $-i0.35^{+3.44}_{-0.11}$	IV	$4440.90^{+4.29}_{-1.20}$ $-i6.68^{+2.96}_{-2.24}$	IV	$4442.96^{+0.62}_{-2.31}$ $-i0.38^{+3.64}_{-0.07}$
	V	$4445.71^{+0.63}_{-4.04}$ $-i2.67^{+0.70}_{-0.80}$	V	$4445.75^{+0.42}_{-1.00}$ $-i0.04^{+1.66}_{-0.04}$	V	$4444.06^{+2.08}_{-1.70}$ $-i2.81^{+0.75}_{-0.77}$
	VII	$4443.93^{+1.58}_{-0.60}$ $-i0.53^{+0.09}_{-0.18}$	VIII	$4441.37^{+4.32}_{-0.47}$ $-i10.80^{+3.57}_{-4.37}$	VII	$4442.23^{+3.45}_{-0.79}$ $-i0.62^{+1.43}_{-0.43}$
	III	$4464.17^{+1.55}_{-6.33}$ $-i5.85^{+6.62}_{-1.92}$
$P_c(4457)$	VII	$4462.56^{+3.07}_{-14.82}$ $-i3.90^{+3.13}_{-3.64}$

TABLE A.3: The pole locations and residues given by our fits. The Riemann sheets with bold type and the ‘*’ symbol means that they are close to the physical sheet. For each pole the locations have difference at the order of keV.

State	Fit	$ g_1 $	$ g_2 $	$ g_3 $
$P_c(4312)$	Fit.1 (RS-V)	$0.29^{+0.03}_{-0.05}$	$2.17^{+0.64}_{-0.66}$	$1.92^{+0.52}_{-0.57}$
	Fit.2 (RS-V)	$0.20^{+0.43}_{-0.04}$	$1.51^{+0.42}_{-0.42}$	$2.29^{+1.17}_{-0.64}$
	Fit.3 (RS-V)	$0.24^{+0.24}_{-0.19}$	$1.35^{+0.21}_{-0.20}$	$0.09^{+0.20}_{-0.09}$
	Fit.A (RS-V)	$0.05^{+0.01}_{-0.02}$	$0.70^{+0.26}_{-0.09}$	$1.19^{+0.19}_{-0.19}$
	Fit.B (RS-V)	$0.01^{+0.01}_{-0.01}$	$0.86^{+0.01}_{-0.01}$	$1.43^{+0.02}_{-0.02}$
	Fit.C (RS-III)	$0.62^{+0.32}_{-0.21}$	$1.79^{+1.41}_{-0.95}$	$2.58^{+3.42}_{-2.58}$
	Fit.C (RS-V)	$0.59^{+0.16}_{-0.12}$	$1.70^{+1.10}_{-0.30}$	$2.45^{+5.31}_{-2.45}$
$P_c(4440)$	Fit.2 (RS-III)	$0.09^{+0.02}_{-0.03}$	$0.34^{+0.15}_{-0.04}$	$0.51^{+0.13}_{-0.12}$
	Fit.3 (RS-III)	$0.03^{+0.04}_{-0.01}$	$0.27^{+0.05}_{-0.05}$	$0.22^{+0.08}_{-0.07}$
	Fit.A (RS-III)	$0.43^{+0.02}_{-0.02}$	$0.83^{+0.13}_{-0.12}$	$1.70^{+0.24}_{-0.21}$
	Fit.B (RS-III)	$0.12^{+0.01}_{-0.01}$	$0.15^{+0.13}_{-0.03}$	$0.77^{+0.16}_{-0.18}$
	Fit.C (RS-III)	$0.10^{+0.05}_{-0.01}$	$0.37^{+0.15}_{-0.09}$	$0.70^{+0.21}_{-0.14}$
$P_c(4457)$	Fit.2 (RS-III)	$0.39^{+0.32}_{-0.07}$	$0.51^{+0.76}_{-0.33}$	$1.48^{+0.89}_{-0.04}$
	Fit.3 (RS-VIII)	$0.69^{+0.32}_{-0.05}$	$0.65^{+0.79}_{-0.65}$	$2.12^{+0.24}_{-0.52}$
	Fit.C (RS-III)	$0.35^{+0.05}_{-0.02}$	$0.51^{+1.10}_{-0.15}$	$1.66^{+2.69}_{-1.00}$

TABLE A.4: The residues of each poles given by our fits. The unit is GeV. We only show the one is closest to the physical region. The notation ‘1, 2 and 3’ denotes the channel that the pole couples to.

being in compatible with that given by the ‘pole counting’ rule. While it has more or less the same order magnitude as that coupling to $\bar{D}^*\Sigma_c$ (g_3). This suggests the strong transition between the $\bar{D}\Sigma_c$ and $\bar{D}^*\Sigma_c$ channels. For the $P_c(4440)$, we find poles in four RSs for all the fits, the same as that of Fits 1, 2 and 3, which fits to the $\cos\theta_{P_c}$ -weighted dataset. As discussed above, it is most likely to be a compact pentaquark. The residue $g_3(P_c(4440))$, except for Fits 3 and A, is smaller than $g_3(P_c(4312))$ and $g_3(P_c(4457))$. This supports that the $P_c(4440)$ is not $\bar{D}^*\Sigma_c$ molecule origin. For the $P_c(4457)$, we do not find poles close to the ‘structure’ as indicated by the data in Fits A and B, while in Fit C the poles are barely close to the physical RS. Indeed, the event shapes of Fit A and C are similar to that of Fit 2, dropping rapidly around the $\bar{D}^*\Sigma_c$ threshold. And in Fit B the line shape has a very clear cusp around the threshold. It confirms that the $P_c(4457)$ is caused by cusp effect at the $\bar{D}^*\Sigma_c$ threshold. However, a component of $\bar{D}^*\Sigma_c$ molecule can’t be excluded, see the $g_3(P_c(4457))$ of Fits 2, 3 and C. It is much larger than $g_{1,2}(P_c(4457))$, though the poles are barely close to the physical RS.

Appendix B: Pole trajectory

In this section we track the trajectories of poles by reducing the magnitude of inelastic channels. That is, we change $K_{ij}(s) \rightarrow \lambda K_{ij}(s)$, where $i \neq j$ and vary λ from one to zero. The trajectories of all the poles of Fit 2 are shown in Fig.4. It should be noticed that the amplitude at $\lambda = 0$ is not physical and the pole could run into weird position. However, as discussed below, it can still give useful hints about the resonances.

$P_c(4312)$

Except for the pole in RS-V, there are three other shadow poles in RS-III, IV and VII. These shadow poles are dragged far away from the pole of RS-V, due to the strong interaction between the pole and the $\bar{D}\Sigma_c$ channel. Finally all of them merge into one ‘destination pole’, which is a resonance ($\sqrt{s_p} = 4428.56 - i112.57$ MeV) in RS-II of $\bar{D}\Sigma$ single channel scattering. Since all the poles in different RSs are originated from $\bar{D}\Sigma$ scattering, it supports the $\bar{D}\Sigma$ molecular picture. This conclusion is consistent with the ‘pole counting’ rule.

$P_c(4440)$

There are four poles nearby $\sqrt{s} = 4440$ MeV in RS-III, IV, V, VII, supporting the non-molecular origin. The poles in RS-III and V merge together at the destination pole ($\sqrt{s_p} = 4441.50 - i1.49$ MeV), a resonance in RS-II of $\bar{D}\Sigma_c$ single channel scattering. And the poles in RS-IV and VII merge together at the destination pole in the real axis ($\sqrt{s_p} = 4444.83$ MeV), a virtual state in RS-II of $\bar{D}^*\Sigma_c$ single channel scattering. Unlike a molecule which couples strongly to the single channel $\bar{D}\Sigma_c$, an elementary particle could couple to multi-channels strongly. See the couplings shown in Table A.4 for the $P_c(4440)$. When the inelastic channels are shut down, the coupled channel scattering is spitted into several single channel scattering, and the destination pole in different single channel behaves differently. The trajectory supports the

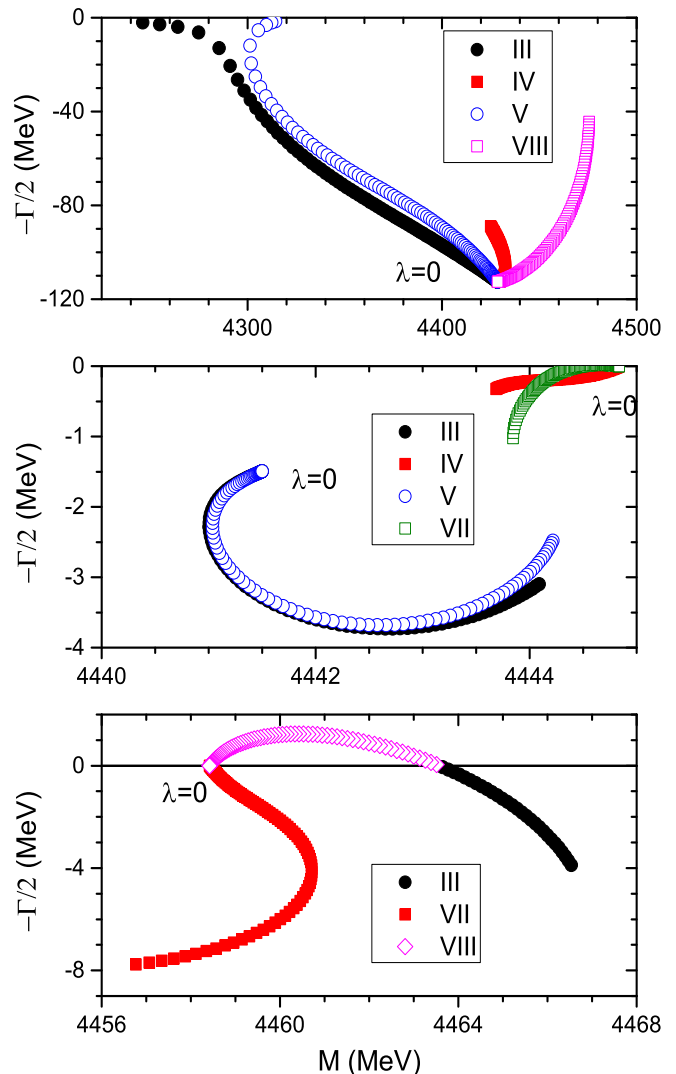


FIG. 4: The trajectories of the poles of Fit 2. λ is varied from 1 to 0, and the step of $\Delta\lambda$ is 0.01.

elementary particle picture (compact pentaquark).

$P_c(4457)$

Only in Fits 2, 3 and C do we find poles close to the $P_c(4457)$ region, and all these poles are not close to the physical sheet. No pole close to the physical region suggests that the structure is generated by the cusp effect. The $P_c(4457)$ pole trajectory of RS-III will go across the cut and get into RS-VIII, finally it meets the pole coming from RS-VII at the real axis. The destination pole ($\sqrt{s_p} = 4458.42$ MeV) lies closely below the $\bar{D}^*\Sigma_c$ threshold ($\sqrt{s_{th3}} = 4459.75$ MeV) and it is the virtual state in RS-II of the $\bar{D}^*\Sigma_c$ single channel. As discussed above, a virtual state close to threshold could also generates ‘cusp’ structure around threshold, see in Ref.[43]. This means that a component of $\bar{D}^*\Sigma_c$ molecule is also possible, and it could be coming from a virtual state origin in single channel. However, our pole analysis reveals that most likely the threshold effect generates the structure of $P_c(4457)$ as shown in the data.

- [1] R. Aaij *et al.* [LHCb Collaboration], “Observation of $J/\psi p$ Resonances Consistent with Pentaquark States in $\Lambda_b^0 \rightarrow J/\psi K^- p$ Decays,” *Phys. Rev. Lett.* **115**, 072001 (2015), arXiv: 1507.03414 [hep-ex].
- [2] F. K. Guo, C. Hanhart, U. G. Meißner, Q. Wang, Q. Zhao and B. S. Zou, “Hadronic molecules,” *Rev. Mod. Phys.* **90**, no. 1, 015004 (2018) arXiv: 1705.00141 [hep-ph].
- [3] Y. R. Liu, H. X. Chen, W. Chen, X. Liu and S. L. Zhu, “Pentaquark and Tetraquark states,” *Prog. Part. Nucl. Phys.* **107**, 237 (2019) arXiv: 1903.11976 [hep-ph].
- [4] N. Brambilla, S. Eidelman, C. Hanhart, A. Nefediev, C. P. Shen, C. E. Thomas, A. Vairo and C. Z. Yuan, “The XYZ states: experimental and theoretical status and perspectives,” arXiv: 1907.07583 [hep-ph].
- [5] R. Aaij *et al.* [LHCb Collaboration], “Observation of a narrow pentaquark state, $P_c(4312)^+$, and of two-peak structure of the $P_c(4450)^+$,” *Phys. Rev. Lett.* **122**, no. 22, 222001 (2019) arXiv: 1904.03947 [hep-ex].
- [6] U. Skerbis and S. Prelovsek, “Nucleon- J/ψ and nucleon- η_c scattering in P_c pentaquark channels from LQCD,” *Phys. Rev. D* **99**, no. 9, 094505 (2019) arXiv: 1811.02285 [hep-lat].
- [7] H. X. Chen, W. Chen and S. L. Zhu, *Phys. Rev. D* **100**, no. 5, 051501 (2019) arXiv: 1903.11001 [hep-ph].
- [8] M. Z. Liu, Y. W. Pan, F. Z. Peng, M. Sánchez Sánchez, L. S. Geng, A. Hosaka and M. Pavon Valderrama, “Emergence of a complete heavy-quark spin symmetry multiplet: seven molecular pentaquarks in light of the latest LHCb analysis,” *Phys. Rev. Lett.* **122**, no. 24, 242001 (2019) arXiv: 1903.11560 [hep-ph].
- [9] F. K. Guo, H. J. Jing, U. G. Meißner and S. Sakai, “Isospin breaking decays as a diagnosis of the hadronic molecular structure of the $P_c(4457)$,” *Phys. Rev. D* **99**, no. 9, 091501 (2019) arXiv: 1903.11503 [hep-ph].
- [10] J. He, “Study of $P_c(4457)$, $P_c(4440)$, and $P_c(4312)$ in a quasipotential Bethe-Salpeter equation approach,” *Eur. Phys. J. C* **79**, no. 5, 393 (2019) arXiv: 1903.11872 [hep-ph].
- [11] Z. H. Guo and J. A. Oller, “Anatomy of the newly observed hidden-charm pentaquark states: $P_c(4312)$, $P_c(4440)$ and $P_c(4457)$,” *Phys. Lett. B* **793**, 144 (2019) arXiv: 1904.00851 [hep-ph].
- [12] C. Fernandez-Ramirez *et al.* [JPAC Collaboration], *Phys. Rev. Lett.* **123**, no. 9, 092001 (2019) arXiv: 1904.10021 [hep-ph].
- [13] Z. G. Wang, “Analysis of the $P_c(4312)$, $P_c(4440)$, $P_c(4457)$ and related hidden-charm pentaquark states with QCD sum rules,” arXiv: 1905.02892 [hep-ph].
- [14] F. L. Wang, R. Chen, Z. W. Liu and X. Liu, “Hidden-charm molecular pentaquarks in the coupled channels of $\Sigma_c^{(*)}(\Lambda_c)-\bar{D}_1(\bar{D}_2^*)$,” arXiv: 1905.03636 [hep-ph].
- [15] J. B. Cheng and Y. R. Liu, *Phys. Rev. D* **100**, no. 5, 054002 (2019) arXiv: 1905.08605 [hep-ph].
- [16] J. J. Wu, T.-S. H. Lee and B. S. Zou, *Phys. Rev. C* **100**, no. 3, 035206 (2019) arXiv: 1906.05375 [nucl-th].
- [17] C. W. Xiao, J. Nieves and E. Oset, *Phys. Rev. D* **100**, no. 1, 014021 (2019) arXiv: 1904.01296 [hep-ph].
- [18] M. B. Voloshin, *Phys. Rev. D* **100**, no. 3, 034020 (2019) arXiv: 1907.01476 [hep-ph].
- [19] Y. J. Xu, C. Y. Cui, Y. L. Liu and M. Q. Huang, “The partial decay width of $P_c(4312)$ as a $\bar{D}\Sigma_c$ molecular state,” arXiv:1907.05097 [hep-ph]. arXiv: 1907.05097 [hep-ph].
- [20] M. Z. Liu, T. W. Wu, M. Sánchez, M. P. Valderrama, L. S. Geng and J. J. Xie, “Spin-parities of the $P_c(4440)$ and $P_c(4457)$ in the One-Boson-Exchange Model,” arXiv: 1907.06093 [hep-ph].
- [21] M. L. Du, V. Baru, F. K. Guo, C. Hanhart, U. G. Meißner, J. A. Oller and Q. Wang, “Evidence that the LHCb P_c states are hadronic molecules and the existence of a narrow $P_c(4380)$,” arXiv: 1910.11846 [hep-ph].
- [22] D. Morgan, “Pole counting and resonance classification,” *Nucl. Phys. A* **543**, 632 (1992).
- [23] L. Y. Dai, X. G. Wang and H. Q. Zheng, *Commun. Theor. Phys.* **57**, 841 (2012) arXiv: 1108.1451 [hep-ph];
- [24] K. L. Au, D. Morgan and M. R. Pennington, “Meson Dynamics Beyond the Quark Model: A Study of Final State Interactions,” *Phys. Rev.* **D35** 1633 (1987); D. Morgan and M.R. Pennington, “New data on the K anti-K threshold region and the nature of the $f_0(S^*)$,” *Phys. Rev.* **D48** 1185 (1993).
- [25] L. Y. Dai, M. Shi, G. Y. Tang and H. Q. Zheng, “Nature of $X(4260)$,” *Phys. Rev. D* **92**, 014020 (2015), arXiv: 1206.6911 [hep-ph].
- [26] X. W. Kang, B. Kubis, C. Hanhart and U. G. Meißner, “ B_{14} decays and the extraction of $|V_{ub}|$,” *Phys. Rev.* **D89**, 053015 (2014, arXiv: 1312.1193 [hep-ph].
- [27] L. Y. Dai and M. R. Pennington, “Comprehensive amplitude analysis of $\gamma\gamma \rightarrow \pi^+\pi^-, \pi^0\pi^0$ and $\bar{K}K$ below 1.5 GeV,” *Phys. Rev. D* **90**, no. 3, 036004 (2014), arXiv: 1404.7524 [hep-ph]; “Pion polarizabilities from $\gamma\gamma \rightarrow \pi\pi$ analysis,” *Phys. Rev. D* **94**, no. 11, 116021 (2016), arXiv: 1611.04441 [hep-ph];
- [28] Z. H. Guo, U. G. Meißner and D. L. Yao, *Phys. Rev. D* **92**, no. 9, 094008 (2015) 1507.03123 [hep-ph];
- [29] Y. H. Chen, M. Cleven, J. T. Daub, F. K. Guo, C. Hanhart, B. Kubis, U. G. Meißner and B. S. Zou, “Effects of Z_b states and bottom meson loops on $\Upsilon(4S) \rightarrow \Upsilon(1S, 2S)\pi^+\pi^-$ transitions,” *Phys. Rev. D* **95**, no. 3, 034022 (2017) arXiv: 1611.00913 [hep-ph].
- [30] L. Y. Dai, J. Haidenbauer and U. G. Meißner, “Re-examining the $X(4630)$ resonance in the reaction $e^+e^- \rightarrow \Lambda_c^+\bar{\Lambda}_c^-$,” *Phys. Rev. D* **96**, no. 11, 116001 (2017) [arXiv:1710.03142 [hep-ph]]. arXiv: 1710.03142 [hep-ph].
- [31] I. Danilkin, C. F. Redmer and M. Vanderhaeghen, *Prog. Part. Nucl. Phys.* **107**, 20 (2019) [arXiv:1901.10346 [hep-ph]]. arXiv: 1901.10346 [hep-ph].
- [32] Q. F. Cao, H. R. Qi, Y. F. Wang and H. Q. Zheng, *Phys. Rev. D* **100**, no. 5, 054040 (2019) doi:10.1103/PhysRevD.100.054040 [arXiv:1906.00356 [hep-ph]]. arXiv: 1906.00356 [hep-ph].
- [33] J. J. Wu, R. Molina, E. Oset and B. S. Zou, *Phys. Rev. Lett.* **105**, 232001 (2010) [arXiv:1007.0573 [nucl-th]]. arXiv: 1007.0573 [nucl-ph].
- [34] J. J. Wu, R. Molina, E. Oset and B. S. Zou, *Phys. Rev. C* **84**, 015202 (2011) arXiv: 1011.2399 [nucl-ph].
- [35] C. W. Xiao, J. Nieves and E. Oset, *Phys. Rev. D* **88**, 056012 (2013) arXiv: 1304.5368 [hep-ph].
- [36] A. V. Manohar and M. B. Wise, “Heavy quark physics,” *Camb. Monogr. Part. Phys. Nucl. Phys. Cosmol.* **10**, 1 (2000).
- [37] G. F. Chew and S. Mandelstam, “Theory of low-energy

- pion pion interactions,” *Phys. Rev.* **119**, 467 (1960).
- [38] B. J. Edwards and G. H. Thomas, “Inelastic Thresholds and Dibaryon Resonances,” *Phys. Rev. D* **22**, 2772 (1980).
- [39] M. Tanabashi *et al.* [Particle Data Group], “Review of Particle Physics,” *Phys. Rev. D* **98**, no. 3, 030001 (2018).
- [40] D. Krupa, V. A. Meshcheryakov and Y. S. Surovtsev, “Multichannel approach to studying scalar resonances,” *Nuovo Cim. A* **109**, 281 (1996).
- [41] L. Y. Dai, X. G. Wang and H. Q. Zheng, *Commun. Theor. Phys.* **58**, 410 (2012) arXiv: 1206.5481 [hep-ph];
- [42] Y. Yamaguchi, H. Garcia-Tecocoatzi, A. Giachino, A. Hosaka, E. Santopinto, S. Takeuchi and M. Takizawa, “Heavy quark spin symmetry with chiral tensor dynamics in the light of the recent LHCb pentaquarks,” arXiv:1907.04684 [hep-ph]. arXiv: 1907.04684 [hep-ph]
- [43] M. Ablikim *et al.* [BESIII Collaboration], “Observation of an anomalous line shape of the $\eta'\pi^+\pi^-$ mass spectrum near the $p\bar{p}$ mass threshold in $J/\psi \rightarrow \gamma\eta'\pi^+\pi^-$,” *Phys. Rev. Lett.* **117**, no. 4, 042002 (2016) arXiv: 1603.09653 [hep-ex];
- [44] L. Y. Dai, J. Haidenbauer and U. G. Meißner, “ $J/\psi \rightarrow \gamma\eta'\pi^+\pi^-$ and the structure observed around the $p\bar{p}$ threshold,” *Phys. Rev. D* **98**, no. 1, 014005 (2018) arXiv: 1804.07077 [hep-ph];
- [45] W. R. Frazer and A. W. Hendry, “S-Matrix Poles Close to Threshold,” *Phys. Rev.* **134**, B1307 (1964).